JOURNAL OF GEOPHYSICAL RESEARCH, VOL. 102, NO. C7, PAGES 15,583–15,593, JULY 15, 1997

A numerical study of wind-induced, near-inertial oscillations over the Texas-Louisiana shelf

Changsheng Chen and Liusen Xie

Department of Marine Sciences, University of Georgia, Athens

Abstract. The wind-induced, near-inertial oscillations over the Texas-Louisiana shelf were studied using a two-dimensional primitive equation model forced by an impulse of the surface wind. Numerical experiments reproduced the cross-shelf structure of observed near-inertial oscillations. For a given spatially uniform impulse of the wind, the model predicted the large near-inertial oscillations that were surface-intensified and characterized by a first baroclinic mode in the vertical. The oscillations reached a maximum kinetic energy near the shelf break and decayed gradually toward the coast but rapidly offshore. The magnitude and cross-shelf distribution of the wind-induced, near-inertial energy changed with wind direction. Effects of nonlinear advection on near-inertial oscillations were largest near the shelf break and decreased both onshore and offshore where the bottom topography was gentle or flat. They were stronger during the wind event and weaker after the wind ceased. Nonlinear interaction of tides and wind was weak on the shelf. However, it tended to provide a positive net contribution to near- inertial currents for both cases where tides were in and out of phase with winds. A simple theory suggests that the cross-shelf variation of near-inertial oscillations was controlled by the cross-shelf gradient of surface elevation and the vertical gradient of Reynolds stress.

1. Introduction

As a major observational component of the Texas-Louisiana Shelf Circulation and Transport Processes Study (LATEX A Program), an array of moored current meters and meteorological buoys was developed in April 1992 to make 3-year measurements of circulation and the near-surface wind field over the LATEX shelf (Figure 1) On the basis of the current and wind data obtained from the first-year measurements, *Chen et al.*[1996] found significant near-inertial oscillations in current data over the LATEX shelf. The amplitude of oscillating currents was about 40 cm/s, which was 3 or 4 times larger than the 40-hour, low-passed currents (Figure 2). The vertical structure of the oscillations was characterized by a first baroclinic mode with a near 180°phase difference between the upper mixed and the lower stratified layers. The oscillations were intermittent with a modulation timescale of about 5 to 10 days. They were surface-intensified and had maximum values near the shelf break, decaying gradually toward the coast but rapidly offshore (Figure 3).

Chen et al. [1996] also reported that the occurrence of near-inertial oscillations of the water currents was closely related to the temporal variation of the surface wind stress. The large oscillations usually kept company with the high-frequency (near-diurnal) variation of the wind stress along with atmospheric frontal passages. On the basis of a simple one-dimensional slab-mixed-layer model forced by the observed surface wind stress, *Chen et al.* [1996] made a prediction of near-inertial currents at mooring stations. They found that the model provided a reasonable simulation when the downward transfer of wind-induced energy through the mixed layer was weak.

The vertical structure of observed near-inertial currents, characterized by the first baroclinic mode with a 180°phase difference above and below the pycnocline, can be simply interpreted as the result of a two-layer system with a solid boundary at the coast. Since the wind-induced, near-inertial oscillating currents were mainly confined in the upper mixed layer, the currents in the lower layer must oscillate in an opposite phase to balance the oscillations in the upper layer and to match the boundary condition of no flux at the coast [*Woods*, 1987; *Chen et al.*, 1996].

However, it is not clear why the observed near-inertial energy peaked near the shelf break and decayed gradually toward the coast and rapidly offshore. *Millot* and *Crépon* [1986] used a two-layer transient model with a flat bottom to examine the influence of the coastal boundary on the cross-shelf structure of wind-induced, near- inertial oscillations. For a given spatially uniform

Paper number 97JC00228.
0148-0227/97/97JC-00228$09.00

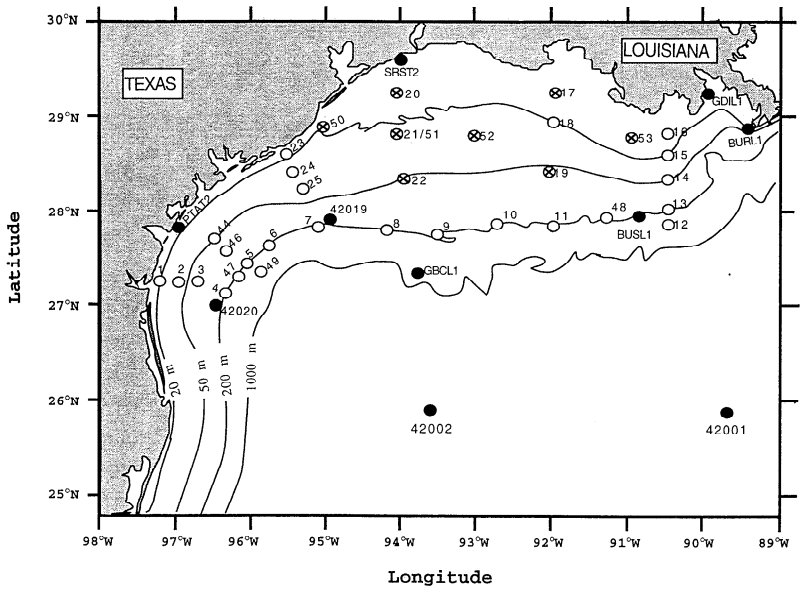

Figure 1. Locations of the LATEX A current meter moorings and meteorological buoys. Open circle, current meter mooring; circle with crosses, current meter mooring with a LATEX A meteorological buoy; solid circle, non-LATEX A meteorological buoy or oil platform.

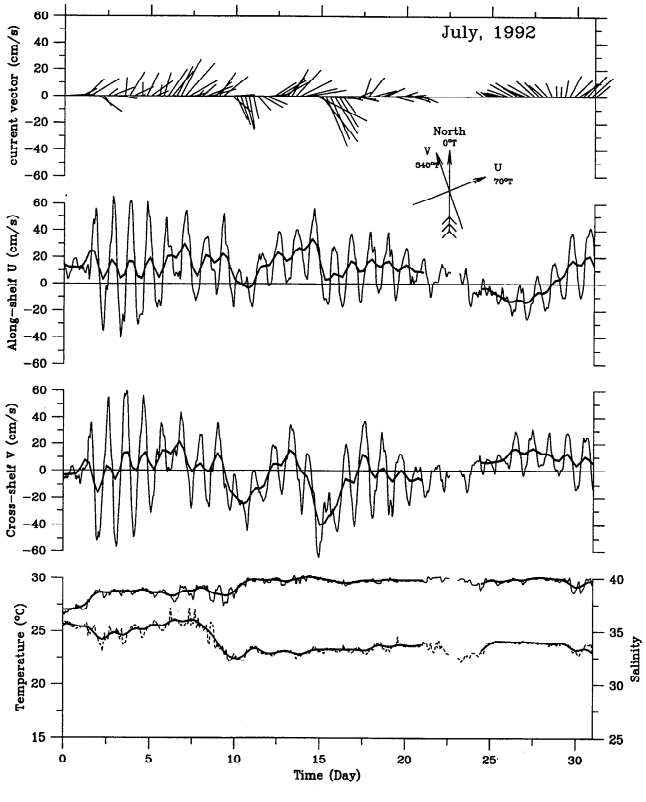

Figure 2. Monthly plots of 40-hour low-passed stick vectors, 3- (thin line) and 40-hour (heavy line) low-passed components of the current, 3- (thin line) and 40-hour (heavy line) low-passed temperature, and 3- (dashed line) and 40-hour (heavy line) low-passed salinity at 12 m for mooring July 13, 1992. The 40-hour low-passed data were obtained by using the 81-point, symmetric low-passed Lanczos filter with half-power point at 40 hours. The low-passed currents obtained by this filter still retained some small signals of the near-inertial motion.

impulse of wind stress, their model shows that the amplitude of the oscillations increased exponentially offshore within a cross-shelf, e-folding scale of the internal radius of Rossby deformation **R**. The e-folding scale of the oscillations was a result of the boundary condition of no flux across the coastline.

Over the LATEX shelf, during spring and summer of 1992, the water was stratified, except near the coast where the water depth was shallower than 10 m. Wind-induced, mixed-layer depth was about 10 to 15 m. **R** was about 5 to 10 km for the ambient strong stratification ($N = 10^{-2}$/s) and a depth range of 20 to 100 m. The fact that the cross-shelf variation scale of the observed oscillations was much larger than R suggests that an additional dynamic process might control the cross-shelf variation of the oscillations. However, this process has not been well explored.

The LATEX shelf is bounded to the north and northwest by the coast. The range of latitude from the coast to the continental slope is from about 29.5°to 27.0°N. Thus the local inertial periods over this shelf range from 24.3 to 26.3 hours close to the K_1 tidal period (23.9 hours) in the north and the O_1 tidal period (25.8 hours) in the south. The tidal currents are only about 2 to 4 cm/s over the LATEX shelf [*Reid* and *Whitaker*, 1981]. However, since the near-inertial period is so close to the diurnal tide, unusually large near-inertial oscillations may occur due to the transfer of inertial energy through nonlinear interaction between wind- and tide-induced currents.

Weller [1982] examined the effect of nonlinear interaction between mean flows on the inertial motion based on the upper ocean velocity field observed at an array of current meters in the northeastern Atlantic Ocean

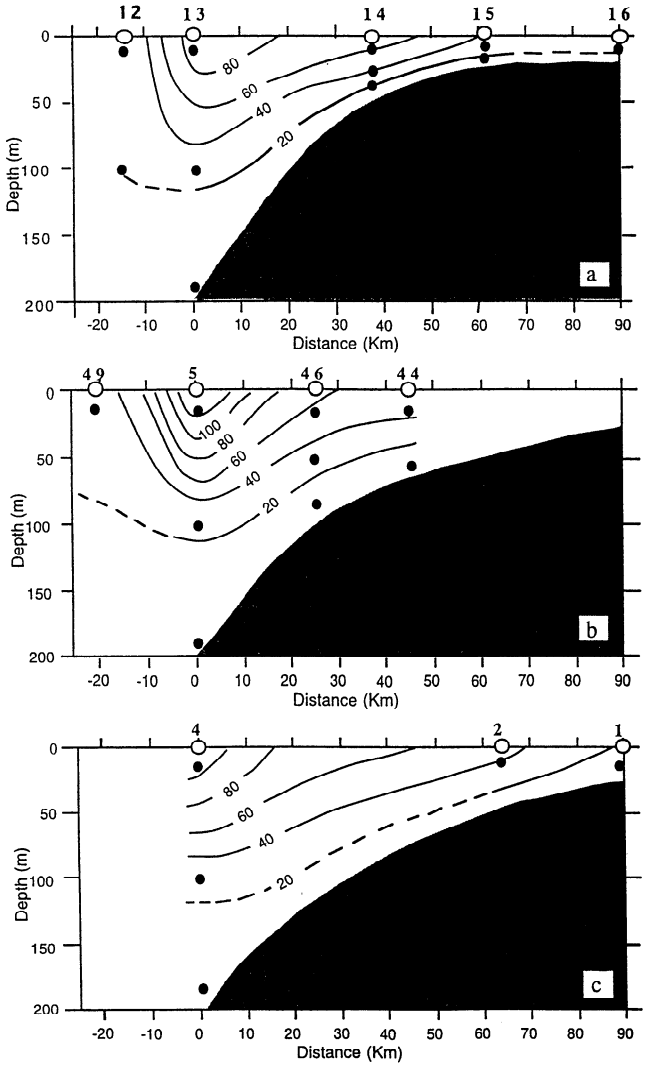

Figure 3. Distributions of the variance of the band-passed, near-inertial currents observed from April 15 to July 22, 1992, at three cross-shelf sections over the LATEX shelf. The contour units are in cm^2/s^2. This figure is from *Chen et al.* [1996].

between Scotland and Iceland. He found that divergence of the quasi-geostrophic flow damped the inertial motion and the vorticity of mean currents shifted the inertial frequency above or below the local inertial frequency. The frequency shift of inertial motions caused by horizontal gradients of the mean velocity field was also pointed out by *Mooers* [1975a, b]. Over the LATEX shelf, the water depth ranges from 20 m near the coast to 200 m at the shelf break over a distance of 150 km. The slope of the bottom topography is about 0.01 across the shelf. Nonlinear advection in such a shallow region may be important for the momentum balance of near-inertial motions. The contribution of nonlinear interaction to the near- inertial oscillations over the LATEX shelf, however, has not been examined.

In this paper, we used a numerical model to explore driving mechanisms for the cross-shelf variation of wind-induced, near-inertial oscillations over the LATEX shelf. To better understand the basic dynamics, we have simplified our study to a two- dimensional (so-called 2-D) problem in which the along-isobath variation for all independent variables was ignored. This paper consists of five sections. Section 2 describes the numerical model. Section 3 represents the model results of near-inertial oscillations under different wind and tidal conditions. In section 4, a diagnostic analysis of the momentum balances is made to examine the dynamic processes that control the cross-shelf structure of near-inertial oscillations. A summary is given in section 5.

2. The Numerical Model

The numerical model used in this study is a modified version of the three- dimensional coastal ocean circulation model developed originally by *Blumberg* and *Mellor* [1987]. This model incorporates the *Mellor* and *Yamada* [1974, 1982] level 2.5 turbulent closure scheme to provide a realistic parameterization of vertical mixing and a free surface to simulate long surface gravity waves. A modification of the stability functions made by *Galperin et al.* [1988] is included in the updated version of the model used in our study.

To better understand the basic dynamic processes that control the cross-shelf variation of near-inertial oscillations, we have simplified our numerical experiments to a 2-D problem involving a cross-shelf slice of the LATEX continental shelf in which along-isobath variation for all independent variables was ignored. The 2-D version of the Blumberg and Mellor model was described in detail by *Chen* and *Beardsley* [1995], and a brief model formulation is given next.

The model consists of momentum, continuity, temperature, salinity, and density equations:

$$\frac{\partial u}{\partial t}+u\frac{\partial u}{\partial x}+w\frac{\partial u}{\partial z}-fv=-\frac{1}{\rho_o}\frac{\partial p}{\partial x}+\frac{\partial}{\partial z}(K_m\frac{\partial u}{\partial z})+F_u \quad (1)$$

$$\frac{\partial v}{\partial t}+u\frac{\partial v}{\partial x}+w\frac{\partial v}{\partial z}+fu=\frac{\partial}{\partial z}\left(K_m\frac{\partial v}{\partial z}\right)+F_v \quad (2)$$

$$\frac{\partial p}{\partial z}=-\rho\, g \quad (3)$$

$$\frac{\partial u}{\partial x}+\frac{\partial w}{\partial z}=0 \quad (4)$$

$$\frac{\partial \theta}{\partial t}+u\frac{\partial \theta}{\partial x}+w\frac{\partial \theta}{\partial z}=\frac{\partial}{\partial z}\left(K_h\frac{\partial \theta}{\partial z}\right) \quad (5)$$

$$\frac{\partial s}{\partial t}+u\frac{\partial s}{\partial x}+w\frac{\partial s}{\partial z}=\frac{\partial}{\partial z}\left(K_h\frac{\partial s}{\partial z}\right) \quad (6)$$

$$\rho_{total}=\rho_{total}(\theta,s) \quad (7)$$

where u, v, and w are the cross-shelf (x), along-shelf

(y), and vertical (z) components of the water velocity; θ is the potential temperature; S is the salinity; P is the pressure; f is the Coriolis parameter; g is the gravitational acceleration; K_m is the vertical eddy viscosity coefficient; and K_h is the thermal vertical eddy friction coefficient. F_u, F_v, and F_θ represent the horizontal momentum and thermal diffusion terms, and ρ and ρ_o are the perturbation and reference density, which satisfy

$$\rho_{total} = \rho + \rho_o \tag{8}$$

The vertical eddy viscosity and diffusion coefficient were calculated using the level 2.5 turbulent closure scheme developed by *Mellor* and *Yamada* [1974, 1982]. The 2-D version of the turbulent closure scheme used in the present study was described in detail by *Chen* and *Beardsley* [1995].

In the absence of surface and bottom heat fluxes, the surface and bottom boundary conditions for the momentum, heat, and salt equations are

$$K_m\left(\frac{\partial u}{\partial x}, \frac{\partial v}{\partial z}\right) = \frac{1}{\rho_o}(\tau_{sx}, \tau_{sy}), \quad \frac{\partial \theta}{\partial z} = \frac{\partial s}{\partial z} = 0,$$
$$w = \frac{\partial \zeta}{\partial t} + u\frac{\partial \zeta}{\partial x}, \quad at \quad z = \zeta(x,t),$$

and

$$K_m\left(\frac{\partial u}{\partial z}, \frac{\partial v}{\partial z}\right) = \frac{1}{\rho_o}(\tau_{bx}, \tau_{by}), \quad \frac{\partial \theta}{\partial z} = \frac{\partial s}{\partial z} = 0,$$
$$w = -u\frac{\partial H}{\partial x}, \quad at \quad z = -H(x)$$

where (τ_{sx}, τ_{sy}) and $(\tau_{bx}, \tau_{by}) = C_d\sqrt{u^2+v^2}(u,v)$ are the x and y components of surface wind and bottom stresses. The surface wind stress was calculated based on the neutral, steady state drag coefficient developed by *Large* and *Pond* [1981]. The drag coefficient C_d was determined by matching a logarithmic bottom layer to the model at a height z_{ab} above the bottom, i.e.,

$$C_d = max\left[k^2/ln\left(\frac{z_{ab}}{z_o}\right)^2, 0.0025\right]$$

where z_o is the bottom roughness parameter, taken here as z_o =0.001 m.

The model domain features a cross-shelf section cut from south to north across the center of the LATEX shelf (Figure 1). The water depth was 500 m off the slope and rapidly decreased to 200 m at shelf break over a distance of about 18 km. Then the depth gradually shallowed to 20 m over a distance of about 150 km from the shelf break to the coast. The numerical model used the σ coordinate transformation defined by $\sigma = (z - \zeta)/(H+\zeta)$. A uniform grid was used in σ. The vertical resolution was $\Delta\sigma = 0.033$ (31 points in the vertical). This corresponded to a vertical Δz of 0.67 m at the 20-m isobath near the coast and 16.7 m at the 500-m isobath off the slope. Nonuniform horizontal grids were used in the cross-shelf direction. The horizontal resolution was 2 km over the shelf extending to 60 km off the slope. Then it increased linearly to 20 km over an interval of 10 grid points outside the domain of interest. The model time step was taken as 142.86 s.

The model was forced by a spatially uniform impulse of the surface wind with a form of Gaussian function, i.e.,

$$W = W_s e^{-\frac{(t-a)^2}{b^2}} e^{-i\hat{\theta}(t)} \tag{9}$$

where W_s is the amplitude of the wind velocity, a is a time of the maximum wind, b is the e-folding time scale, and $\hat{\theta}(t)$ is the direction of the wind, which was taken as 0° for cross-shelf wind, 90° for along-shelf wind, and $2\pi(t-24)/T$ (from 0°to 360°) for rotating wind. The model was run for a period of 15 days. The wind was imposed at the twenty-fourth hour, at a time when the model was fully ramped up from initial conditions (note that when the tidal forcing was included, the model needed to be ramped up). Here a was taken as 36 hours and b was 3 hours. T was the time interval during which the wind blew. In our experiments, it was taken as 24 hours.

The model was run as an initial value problem with homogeneous and stratified cases. The initial distribution of salinity was given by a vertical profile of observed data taken at the 500-m isobath during the spring 1992 LATEX A hydrographic cruise. The salinity was 36.21 at the surface and decreased to 34.91 at 500 m (note that the model also was run for a given initial distribution of salinity as a linear function of z with 36.21 at the surface and 34.91 at 500 m. Results for near-inertial currents were identical). The initial distribution of temperature was simply specified as a linear function of z with 25.5°at the surface and 7.5°at the 500 m. In each case, numerical experiments were conducted for cross-shelf, along-shelf, and rotating winds with a maximum wind speed of 5, 10, and 15 m/s, respectively. A gravity wave radiation boundary condition, plus a sponge layer, was specified at the open boundary to allow the energy to leave the computational domain with minimum reflection [*Chapman*, 1985].

To compare with observations described by *Chen et al.* [1996], we adopted the same definition for near-inertial currents: the band-passed currents filtered by a digital, nonphase distorted filter with a bandwidth of admitting periods from 22 to 28 hours. The variance was estimated based on the band-passed currents with a time range of 14 days counted from starting time of the wind to the end of the model run.

3. Model Results

Homogeneous Case

Figure 4 shows the variance of near-inertial motions for the homogeneous cases forced by cross-shelf (Figure 4a), along-shelf (Figure 4b), and rotating (Fig-

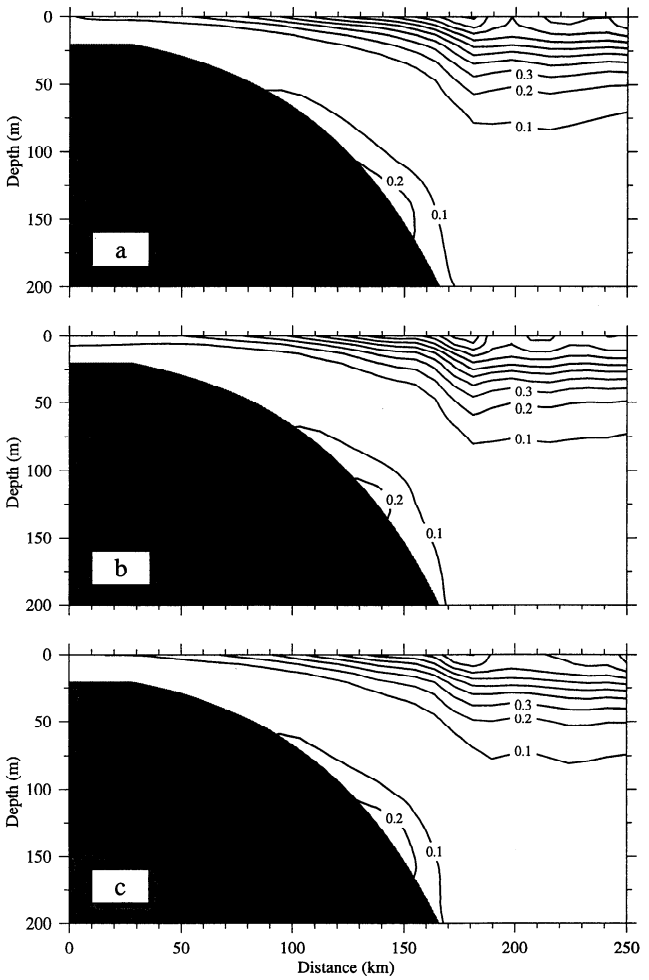

Figure 4. Distributions of the variance of the band-passed, near-inertial currents for the homogeneous cases with the (a) cross-shelf, (b) along-shelf, and (c) clockwise rotating wind forcings. The contour interval is 0.1 cm^2/s^2.

ure 4c) winds.Figure 4 For a given maximum wind speed of 10 m/s, the model results for three cases showed a maximum of the variance of near-inertial currents near the 200-m isobath at the shelf break. The variance decreased gradually onshore from the shelf break but remained almost constant offshore. The vertical thickness of near-inertial currents increased offshore from the coast to the shelf break and then became constant off the slope. The maximum depth of near-inertial oscillations was about 75 m from the surface in the off- slope region. In addition to the oscillations near the surface, the model also showed near-inertial energy near the bottom on the slope for all three cases. Such bottom oscillations were about 180° out of phase with those near the surface.

Wind-induced, near-inertial currents were significant during the first 2 days after the wind blew, and then they decayed rapidly with time. For the case forced by the along-shelf wind, as an example, the maximum value of near-inertial currents was about 3 cm/s at a time when the wind vanished, and it decreased to 0.1 cm/s after 2 days. The maximum variance at the shelf break was only 1.18 cm^2/s^2, 1.28 cm^2/s^2, and 0.98 cm^2/s^2 for the cases forced by the cross-shelf, along-shelf, and rotating (clockwise) winds, respectively.

The existence of near-inertial oscillations near the bottom on the slope was associated with the wind-induced energy dissipation in the sloping bottom boundary layer. In the homogeneous case, the currents responded almost instantaneously to local surface wind stress in shallow depths because of strong turbulent mixing. In the middle and outer shelves, where the depth was greater, friction became weaker and the downward transfer of wind momentum took longer. The currents in these regions therefore responded more directly to the Ekman pumping of surface wind stress [*Csanady*, 1974]. In a linear system, the cross-shelf volume transport can be expressed as a sum of surface Ekman (U_e), interior (U_i), and bottom Ekman (U_b) transports. For the case in which the cross-shelf scale of the motion is smaller than the external Rossby radius ($\sqrt{gH}/f$), the cross-shelf volume transport will be approximately equal to zero because of no flux boundary condition at the coast. On the basis of this assumption, the cross- shelf bottom Ekman transport must be equal in magnitude and be opposite in direction to cross-shelf surface Ekman and interior transports. Since the oscillations were weak in the interior near the shelf break in the homogeneous case, the water in the bottom Ekman layer must oscillate with an opposite phase to that in the surface Ekman layer. In this case, the bottom Ekman layer acted as a sink for the input of wind momentum at the surface.

Stratified Case

When stratification was included, the near-inertial oscillations became much stronger (Figure 5). For a given maximum wind speed of 10 m/s in the cross-shelf direction, the near-surface inertial currents near the shelf break increased to about 37 cm/s during the wind event and then oscillated with an amplitude of about 10 cm/s after the wind relaxed (Figure 5c). The oscillating currents near the coast were about 25 cm/s at a time of maximum wind, and then they rapidly decayed after the wind ceased (Figure 5a). The amplitude of near-inertial currents near the outer slope was about 15 cm/s during the wind event and gradually decreased to about 7 cm/s over a time interval of 10 days after the wind stopped (Figure 5d).

The amplitude of near-inertial currents decreased with depth. An example is shown in Figure 6 for the case forced by the cross-shelf wind. The maximum amplitude of oscillating currents at the 106-m isobath, 128 km off the coast, was about 38 cm/s at the depth of 2 m below the surface. It decreased with depth to about 3 cm/s at the depth of 83 m. The vertical phase distribution of near-inertial currents was characterized by

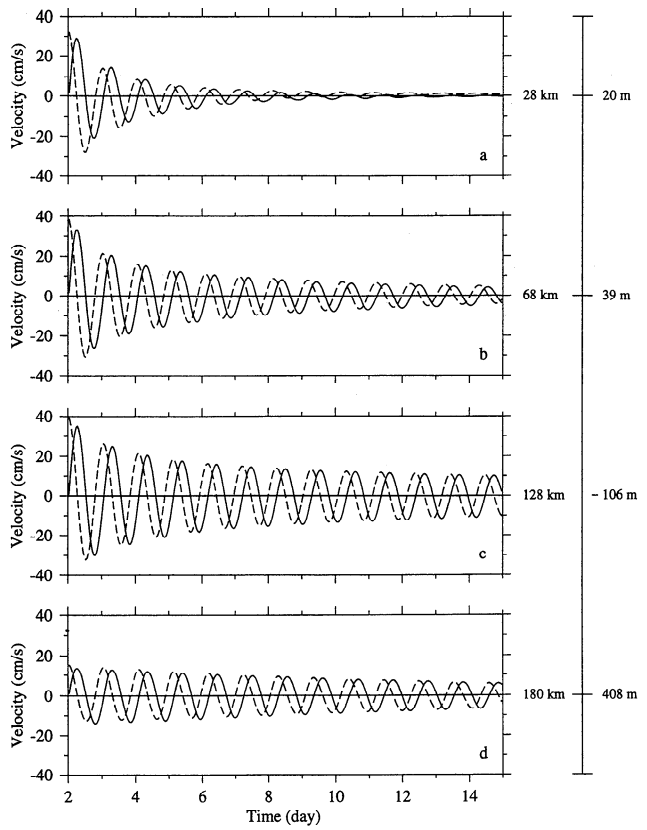

Figure 5. Time series of the band-passed, near-inertial currents at the surface at four locations: 28, 68, 128, and 180 km from the coast. Solid and dashed lines are the cross-shelf (u) and along-shelf (v) velocity components, respectively. The digital number on the right side indicates the distance (km) from the coast and the water depth (m) at that location.

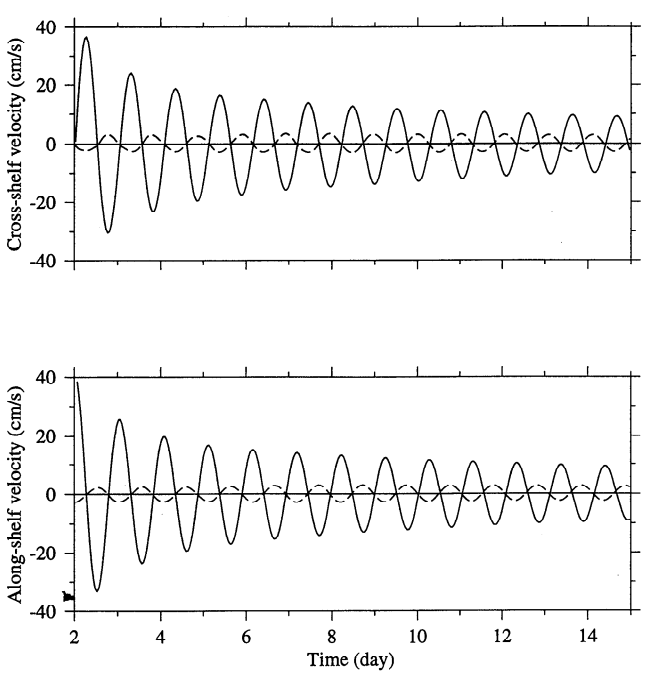

Figure 6. Time series of the band-passed, near-inertial currents at depths of 1.8 m (solid line) and 83 m (dashed line) at a location with a distance of 128 km from the coast and a water depth of 106 m.

a first baroclinic mode in mixed and stratified layers. The oscillations in the lower stratified layer were about 180o out of phase with those near the surface.

The spatial difference of near-inertial energy was clearly seen in the cross-shelf distribution of the variance calculated for band-passed, near-inertial currents. As an example, for the case forced by the cross-shelf wind, the variance reached a maximum of 234 cm^2/s^2 at near the 200-m isobath, 160 km off the coast, and decayed gradually onshore but rapidly offshore (Figure 7). It decreased to zero at the coast over a distance of 160 km and to 100 cm^2/s^2 at a 500-m isobath, over a distance of 20 km from the shelf break (Figure 8). The variance of near-inertial currents also decreased with depth. Strong near- inertial energy was mainly located in the upper 20 m from the surface, even though it did penetrate into the deeper region along the slope of the bottom over the continental shelf (Figure 7a).

The amplitude of near-inertial oscillations changed with wind direction. For a given maximum wind speed

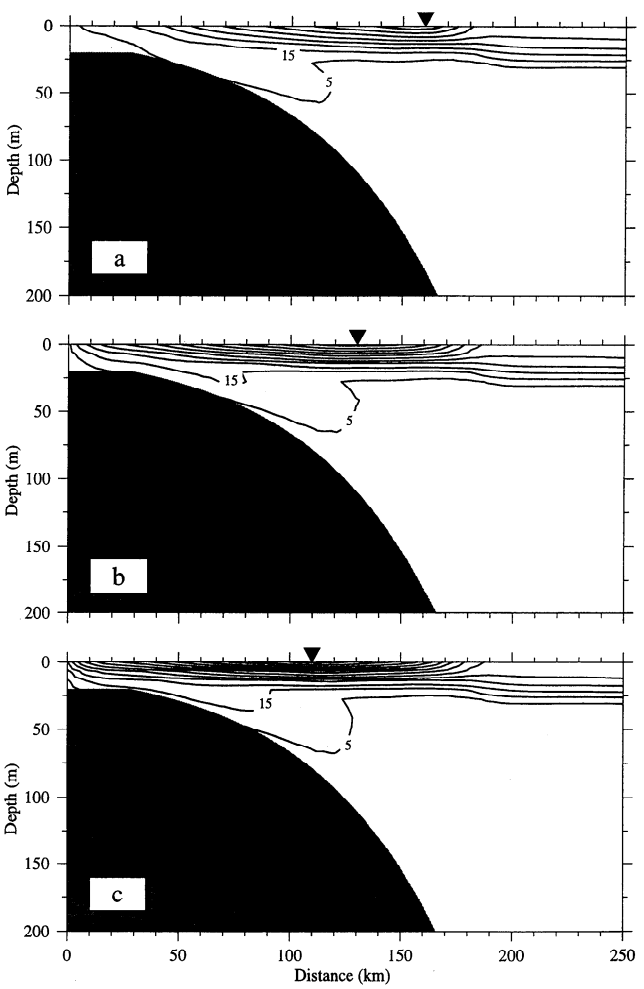

Figure 7. Distributions of the variance of the band-passed, near-inertial currents for the stratification cases with the (a) cross-shelf, (b) along-shelf, and (c) clockwise rotating winds. The contour interval is increased with an unit of 5(n+1) cm2 /s2, n=1, 2,....., 12. The solid inverted triangle indicates the location of the maximum variance.

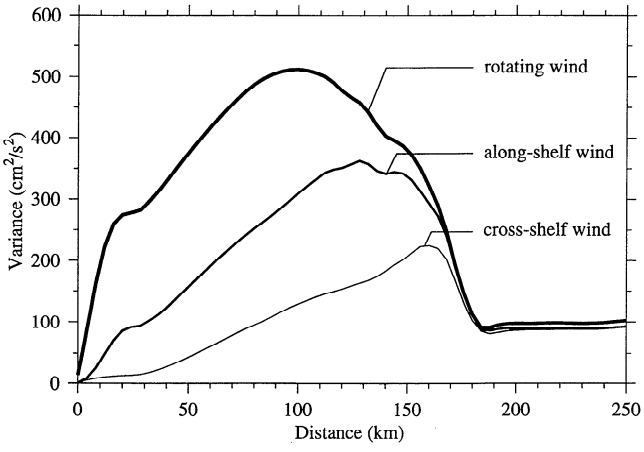

Figure 8. Distributions of the surface variance of the band-passed, near-inertial currents for the stratification cases with the cross-shelf, along-shelf, and clockwise rotating winds.

of 10 m/s, the maximum variance of inertial currents was 363 cm^2/s^2 in the case forced by the along-shelf wind, which was 129 cm^2/s^2 larger than that in the case forced by the cross-shelf wind. The maximum variance increased to 512 cm^2/s^2 in the case forced by the rotating wind. The cross-shelf structure of near-inertial oscillations remained almost unchanged for different wind directions. However, the location of the maximum variation of near-inertial motions shifted onshore to the 110-m isobath, 130 km off the coast in the case forced by the along-shelf wind, and to the 80-m isobath, 100 km off the coast in the case forced by the rotating wind.

The amplitude of near-inertial currents increased with the magnitude of the wind speed. An example is given in Figure 9. For the case forced by the along-shelf wind, the maximum variance of near-inertial currents was only about 10 cm^2/s^2 for a maximum wind speed of 5 m/s. The variance increased to 363 cm^2/s^2 and 1008 cm^2/s^2 as the maximum wind speed increased to 10 m/s and 15 m/s, respectively.

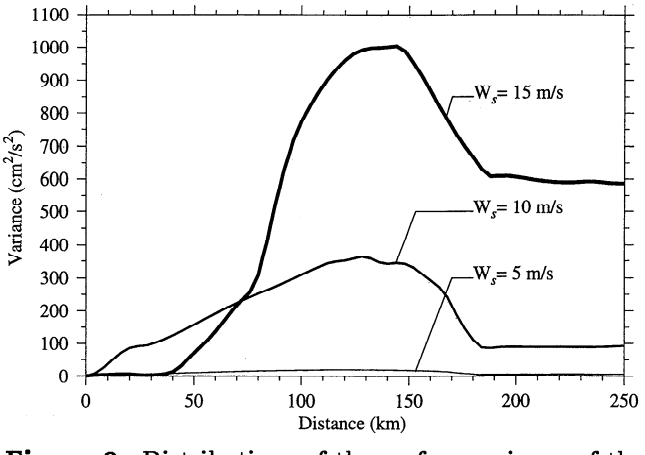

Figure 9. Distributions of the surface variance of the band-passed, near-inertial currents for the stratification cases forced by the along-shelf wind with a maximum wind speed of 5, 10, and 15 m/s.

The location of maximum variance remained almost unchanged with wind speed. The cross-shelf gradient of the variance, however, was significantly increased as the wind became stronger. For a maximum wind speed of 10 m/s, the variance of near- inertial currents tended to increase gradually to a maximum over a distance of 130 km from the coast. As the wind increased to 15 m/s, however, the variance remained near zero within 40 km off the coast and then rapidly increased to 1008 cm^2/s^2 over a cross- shelf distance of about 90 km.

Effects of Nonlinear Interactions

The model results showed that effects of nonlinear interactions on near-inertial oscillations varied with location and time (note that the linear case was defined as the case in which the advection terms in momentum equations were zero). They were largest near the shelf break and decreased both onshore and offshore where the slope of the bottom topography was gentle or flat. The nonlinear effects were stronger during the wind event and weaker after the wind ceased. An example is shown in Figure 10 near the shelf break for both linear and nonlinear cases forced by the along-shelf wind. Near-inertial oscillations were significantly intensified due to the nonlinear advection during the wind event. At the end of the second day, when the wind just ceased, the near-inertial currents in the nonlinear case were about 20 cm/s larger than those in the linear case. Nonlinear effects became weaker after the wind vanished, and the oscillations were almost linear after 8 days.

No significant phase shift was observed in our model results, even though the nonlinear advection was rela-

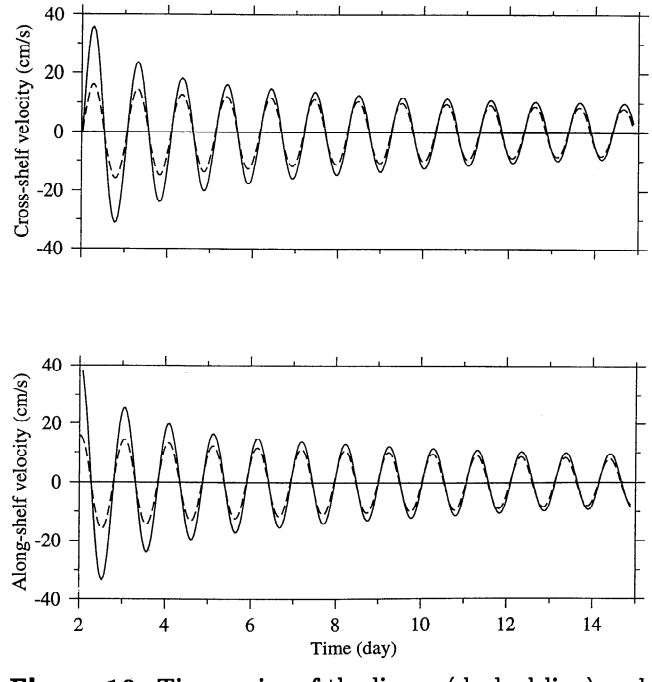

Figure 10. Time series of the linear (dashed line) and nonlinear (solid line) band-passed, near-inertial currents at the surface.

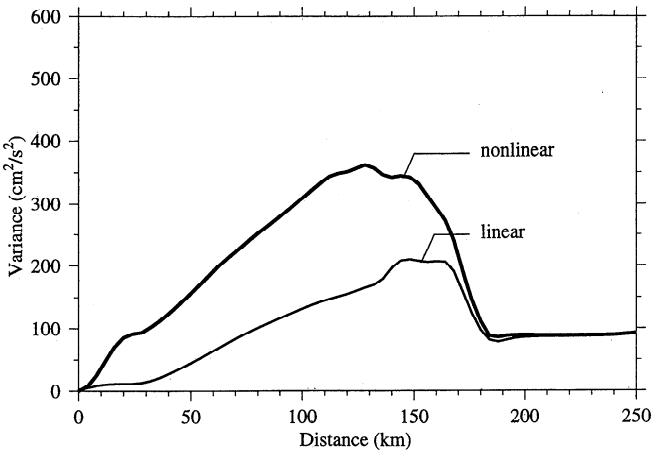

Figure 11. Distributions of the variance of the linear and nonlinear band-passed, near- inertial currents at the surface for the stratification case forced by the along-shelf wind.

tively strong during the wind event. The basic cross-shelf structure of the variance of near-inertial currents was very similar in both nonlinear and linear cases despite a large difference in amplitudes (Figure 11). For a given maximum wind speed of 10 m/s, the maximum variance of near-inertial currents in the linear case was only about 200 cm^2/s^2, 163 cm^2/s^2 less than that in the nonlinear case. Off the slope, where the bottom topography was flat, the variances of near-inertial currents were almost identical for both linear and nonlinear cases.

Effects of tidal currents

Reid and *Whitaker* [1981] numerically simulated the astronomical tides in the Gulf of Mexico. By tuning the model to best fit the available coastal tidal data, they provided the cotidal charts of semidiurnal and diurnal tides for the entire Gulf. The cotidal charts for diurnal O_1 and K_1 showed that at the central LATEX shelf, the amplitude of the tidal elevation increased toward the coast with the same phase. The computed sea level at about the 500-m isobath, near the edge of the slope, was about 14 cm, and it increased to 18 cm near the coast. On the basis of this information, we have forced the model with a barotropic K_1 tidal elevation with an amplitude of 14 cm at the southern open boundary. The wind forcing was imposed after the tidal currents reached a state of quasi-equilibrium.

For the stratification case forced only by the tide, the model predicted standing, wave-like, diurnal oscillating currents over the shelf. The oscillating currents were intensified near the bottom on the slope, leading to an axis of the maximum currents parallel to the slope. The magnitude of currents was less than 0.5 cm/s off the slope and reached a maximum of 2.4 cm/s at the surface on the 35-m isobath, 55 km off the coast.

The cross-shelf distribution of the oscillating tidal energy was represented here by the variance calculated for the K_1 tidal currents (Figure 12). The variance was intensified at the surface within the inner shelf where the water depth was less than 50 m and near the bottom of the slope. The maximum variance was about 5.6 cm^2/s^2 at the surface over the inner shelf, 55 km off the coast.

Our model results showed that effects of diurnal tidal currents on the wind- induced, near-inertial currents changed with the phase of wind forcing. Examples are shown in Figures 12 and 13 for the case forced by the along-shelf wind. When the wind was in phase with diurnal tidal currents, the interaction between the wind- and tide- induced currents enhanced the near-inertial oscillations over the shelf. The maximum variance of the near-inertial currents increased to 471 cm^2/s^2, about 108 cm^2/s^2 larger than that in the case with no tide (Figure 13). Contributions of tidal currents on near-inertial oscillations also varied across the shelf.

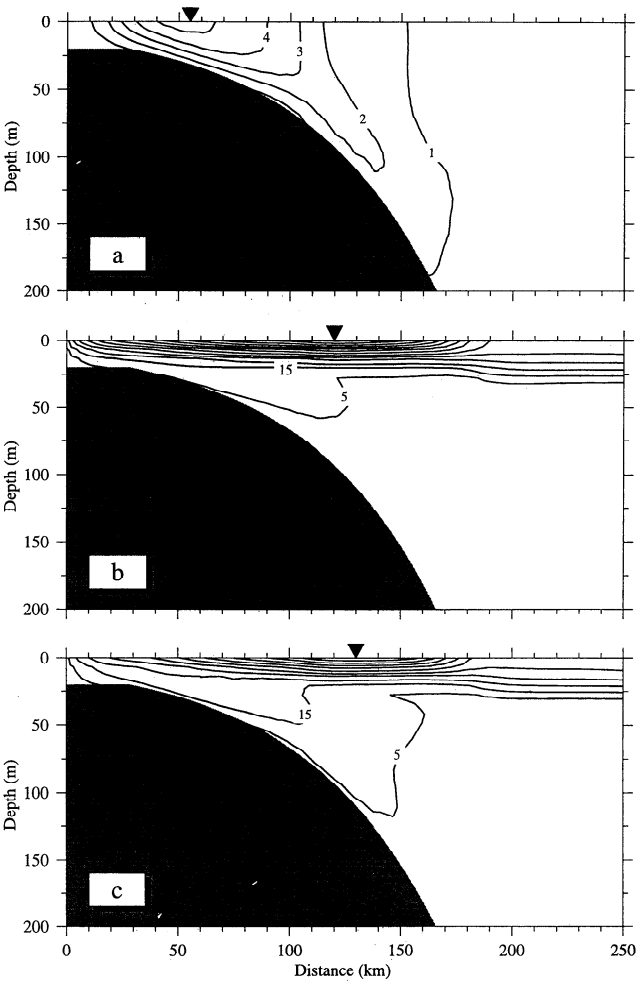

Figure 12. Distributions of the variance of the (a) stratified K_1 tidal currents and band-passed, near-inertial currents for the stratification case forced by the along-shelf wind with the (b) same and (c) opposite phase as the K_1 tidal current. The contour interval is 1.0 cm^2/s^2 for the case with only tidal forcing and 5(n+1) cm^2/s^2, n=1, 2,...., 12 for the case with tide plus wind forcing. The solid inverted triangle indicates the location of the maximum variance.

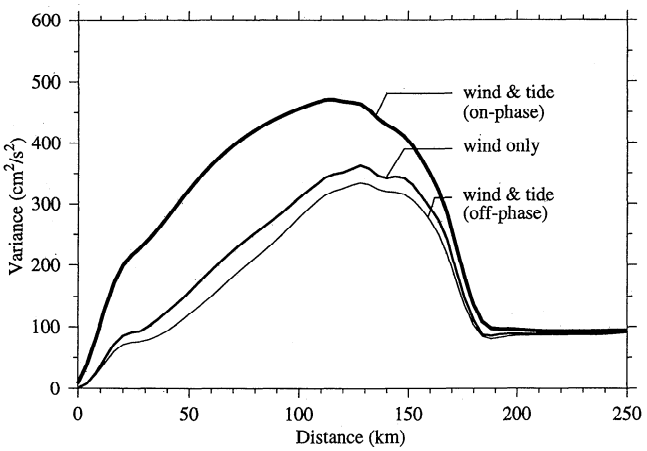

Figure 13. Distributions of the surface variance of the band-passed, near-inertial currents for three stratification cases: (1) the only along-shelf wind, (2) the along-shelf wind plus a same phase K_1 tidal current, and (3) the along-shelf wind plus an opposite phase K_1 tidal current.

They were larger over the shelf where the nonlinear advection of near-inertial currents was strong (see Figure 11) and weaker off the slope where the oscillations were almost linear.

When the wind phase was opposite the phase of diurnal tidal currents, the interaction of wind- and tide-induced currents tended to reduce the amplitude of near- inertial oscillations over the shelf, where nonlinear advection of currents was strong (Figure 11). The maximum variance of near-inertial currents was about 338 cm^2/s^2, which was about 25 cm^2/s^2 less than that in the case with no tide. In this case, the inclusion of the tide had a slight influence on the near-inertial energy.

Interaction between tides and winds was through a weak nonlinear process. This feature can be seen from a simple scaling analysis. In a nonlinear system driven by both wind and tidal forcings, the near-inertial current U_I can be rewritten as a sum of $U_w + U_T + U_{w+T}$, where U_w and U_T are the wind- and tide-induced inertial currents and U_{w+T} is the inertial current produced by nonlinear interaction between tides and winds. For the case where the tide was in phase with the wind, U_I was found to be 21.7 cm/s for a maximum variance of 471 cm^2/s^2. The mean currents of U_w and U_T, estimated from the cases forced by tide and wind separately, were about 19.1 cm/s and 1.2 to 1.7 cm/s for the maximum variances of 363 cm^2/s^2 and 1.5 to 3.0 cm^2/s^2. U_{w+T}, as a result of $U_I - U_w - U_T$, equaled 0.9 to 1.4 cm/s, one order smaller than either U_I or U_w but the same order as the magnitude of tidal currents.

Similarly, when the tidal phase was opposite the wind phase, U_I was 18.4 cm/s for a maximum variance of 338 cm^2/s^2. U_{w+T}, as a result of $U_I - U_w + U_T$, equaled 0.5 to 1.0 cm/s, half as large as tidal currents and 1 order smaller than either U_I or U_w. In both cases where the wind was in and out of phase with the tide, the nonlinear interaction tended to provide a positive contribution to the near-inertial energy over the shelf.

Comparison with observations

Our model results are qualitatively consistent with observations described by *Chen et al.* [1996]. The model does predict the near- inertial oscillations that are intensified near the surface and characterized by a first baroclinic mode in the vertical. Similar to the observations, the model oscillations have a maximum kinetic energy near the shelf break and decay gradually toward the coast but rapidly offshore.

On the Basis of a Rayleigh criterion, *Chen et al.* [1996] attempted to use the harmonic analysis method to remove the diurnal tidal signals from a long time series of current meter data obtained from the LATEX moorings. They found that the estimated bias of diurnal tidal currents decreased as the length of data records increased. However, the estimated phases of diurnal tidal currents were very sensitive to the data length. Our model results showed that the dynamic processes of wind- and tide-induced near-inertial currents were weakly and nonlinearly coupled in this region. The near-inertial currents produced by the nonlinear interaction between tide and wind were of the same order as tidal currents. Therefore a large uncertainty in the estimated phase of diurnal tidal currents found from *Chen et al.* [1996] data analysis was likely due in part to such a weak nonlinear nature of near-inertial oscillations over the LATEX shelf.

4. Discussion

A diagnostic analysis for the momentum equations is made here to study the driving mechanism for the cross-shelf variation of near-inertial oscillations. The fact that the cross-shelf structure of near-inertial energy remained almost unchanged in the linear system without nonlinear advection allows us to simplify our analysis using a linear model (Figure 11).

In a linear system with no horizontal diffusion, the 2-D momentum equations (1) and (2) can be rewritten with a complex form as

$$\frac{\partial U}{\partial t} + ifU = -\frac{1}{\rho_o}\frac{\partial p}{\partial x} + \frac{\partial \tau}{\partial z} \qquad (10)$$

where $U = u + iv$ and $\tau = \tau_x + i\tau_y$ are the complex forms of the velocity and Reynolds stress. Here τ_x and τ_y are the cross-shelf (x) and along-shelf (y) components of τ. A solution for (10) can be obtained with a form of

$$U = \int_0^t \left(-\frac{1}{\rho_o}\frac{\partial p}{\partial x} + \frac{\partial \tau}{\partial z}\right) e^{if(t'-t)}dt' \qquad (11)$$

where U is initialized as zero. This solution suggests that the cross-shelf distribution of near-inertial oscillations is controlled by the cross-shelf pressure gradient and the vertical gradient of Reynolds stress.

For the homogeneous case, (11) can be simplified as

$$\bar{U} = \int_0^t (-g\frac{\partial \zeta}{\partial x} + \frac{\tau_s - \tau_b}{h(x)})e^{if(t'-t)}dt' \qquad (12)$$

where $\bar{U}$ is the complex form of vertically averaged inertial currents, ζ is the surface elevation, τ_s and τ_b are the complex forms of the surface wind stress and the bottom stress, and $h(x)$ is the water depth. Equation (12) suggests that for a given spatially uniform τ_s, the cross-shelf structure of $\bar{U}$ is controlled by $\partial\zeta/\partial x$, τ_b, and $h(x)$. The maximum amplitude of $\bar{U}$ should occur at a location where the derivative of $[g\partial\zeta/\partial x + \tau_b/h(x)]$ equals zero.

For the stratified case, the hydrostatic approximation simplifies the pressure p to be a sum of barotropic ($\rho_o g\zeta$) and baroclinic (p^*) pressures. Equation (11) suggests that the maximum amplitude of inertial oscillating currents at a given depth should occur at a location where the magnitude of the resultant forcing, due to the sum of the cross-shelf gradients of surface elevation, the baroclinic pressure gradient, and the vertical gradient of Reynolds stress, reaches a maximum value.

For example, Figure 14 shows a time sequence of the cross-shelf distributions of the near-surface forcing [i.e., right side of (11)] for the case of an along-shelf impulse of wind stress. In this case, a spatially uniform wind, which was imposed at the twenty-fourth hour, reached a maximum speed of 10 m/s 12 hours later. About 5 hours after the maximum wind (at 40.8 hours), a sharp peak in the resultant forcing occurred about 20 km off the coast. The peak moved continuously offshore during the wind event, while the magnitude of this peak decreased as the wind decreased (Figure 14a). After the wind ceased, the peak remained near the shelf break between 140 and 160 km off the coast (Figure 14b).

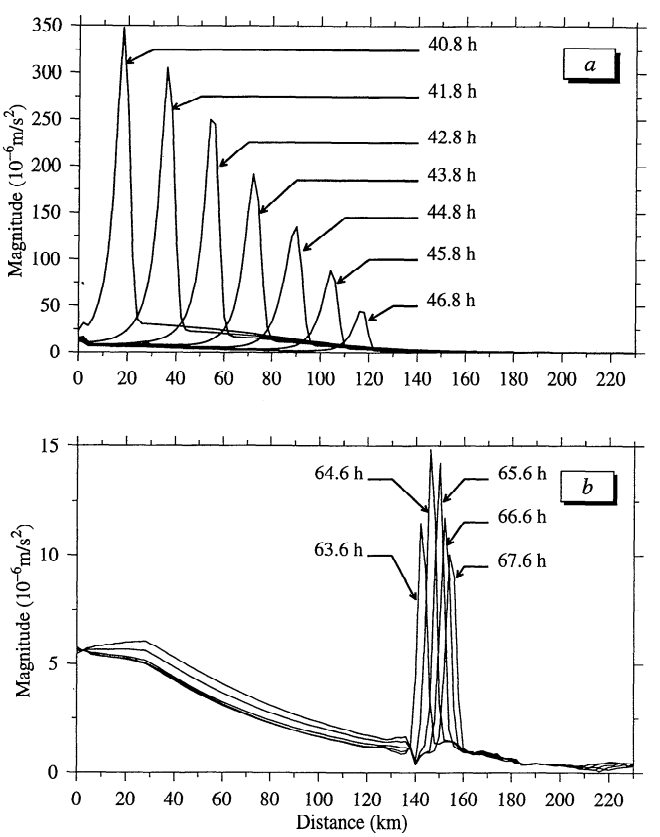

Figure 14. Time sequence of the cross-shelf distribution of the resultant forcing of the cross-shelf gradient of surface elevation and the vertical shear of Reynolds stress near the surface for the case of an along-shelf impulse of wind stress.

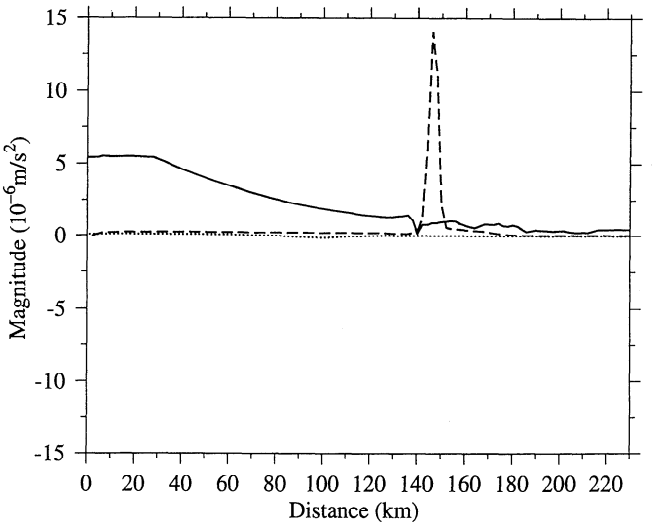

Figure 15. Cross-shelf distributions of the cross-shelf gradient of surface elevation (solid line), the cross-shelf (dashed line), and the along-shelf (dotted line) components of the vertical gradient of Reynolds stress at the first grid point below the surface at 66.5 hours.

Figure 15 shows the cross-shelf distribution of $-g\partial\zeta/\partial x$, $\partial\tau_x/\partial z$ and $\partial\tau_y/\partial z$ at 66.5 hours, about 18 hours after the wind ceased. The vertical gradient of Reynolds stress was estimated at the first grid point below the surface. Since the wind stress vanished at this time, the vertical gradient of Reynolds stress at the first grid point was equal to the product of the velocity shear and the eddy diffusion coefficient. We excluded the baroclinic pressure gradient in our analysis because it was negligible near the surface.

The vertical gradient of along-shelf stress ($\partial\tau_y/\partial z$) decreased rapidly after the wind stopped. During the period of free oscillations, the cross-shelf structure of oscillating currents over the inner and middle shelves was controlled by the cross-shelf gradient of surface elevation ($-g\partial\zeta/\partial x$), while it was controlled by the vertical gradient of cross-shelf stress ($\partial\tau_x/\partial z$ or $-\tau_x/\Delta z$) at the shelf break. The cross-shelf gradient of surface elevation remained almost constant near the coast and then gradually decreased seaward. The vertical gradient of cross-shelf stress was close to zero over the inner and middle shelves but rapidly increased and then decreased at the shelf break. The cross- shelf distribution of these two forces was consistent with the cross-shelf structure of the variance of near-inertial currents, which gradually increased in the seaward direction across the

inner and middle shelf, reaching a maximum at the shelf break (see Figure 11).

The fact that the model results were consistent with the linear theory suggests that the cross-shelf gradient of surface elevation and the vertical gradient of Reynolds stress controlled the cross-shelf structure of near-inertial oscillations. The model results indirectly imply that both the coastal boundary and variable bottom topography play important roles in the cross-shelf variation of near-inertial motions.

5. Conclusions

Numerical experiments with a two-dimensional coastal ocean circulation model reproduced the cross-shelf structure of wind-induced, near-inertial oscillations observed by *Chen et al.* [1996]. For a given spatially uniform impulse of the wind, the model predicted the large near-inertial oscillations that were surface-intensified and characterized by a first baroclinic mode in the vertical. The oscillations reached a maximum kinetic energy near the shelf break and decayed gradually toward the coast but rapidly offshore.

The magnitude and cross-shelf variation of the wind-induced, near-inertial energy changed with wind directions. In the stratified case, the location of maximum variance of near-inertial currents shifted onshore as the wind turned from a cross-shelf direction to an along-shelf direction or rotated clockwise. The amplitude of the oscillations was small for a cross-shelf wind, larger for an along-shelf wind, and largest for a rotating (clockwise) wind.

Effects of nonlinear advection on the near-inertial oscillations varied with location and time. They were largest near the shelf break and decreased both onshore and offshore where the bottom topography was gentle or flat. Nonlinear advection tended to intensify the near-inertial oscillations. It was stronger during the wind event and weaker after the wind ceased. Nonlinear interaction of tides and winds was weak on the shelf. However, it tended to provide a positive net contribution to the near-inertial energy for both cases where the tide was in and out of phase with the wind.

A linear theory shows that the cross-shelf variation of near-inertial oscillations is controlled by the cross-shelf gradient of surface elevation and vertical gradient of Reynolds stress. The maximum variance of the near-inertial currents occurs at a location where the magnitude of the resultant forcing, due to a sum of the cross-shelf gradient of surface elevation and the vertical gradient of Reynolds stress, reaches a maximum value. This theory is consistent with our model results, which imply that near-inertial oscillations over the continental shelf are controlled by the presence of the coast and topography.

Acknowledgments. This research was supported by the Office of Naval Research (ONR) under grant N00014-93-1-0513 and subcontract RR50905F to University of Georgia. Also, we want to thank Bob Reid and two anonymous reviewers for their valuable comments and George Davidson for his editorial help on this manuscript. Observed data used in this study were collected during the Louisiana-Texas Shelf Circulation and Transport Process Study (LATEX A) at Texas A&M University. The LATEX A program is supported by the Minerals Management Services of the U.S. Department of the Interior, under OCS contract 14-35-0001-30509.

References

Blumberg, A. F., and G. L. Mellor, A description of a three-dimensional coastal ocean circulation model, *In Three-Dimensional Coastal Ocean Models, Coastal Estuarine Sci.*, vol. 4, edited by N. S. Heaps, pp. 1-6, AGU, Washington D.C. 1987.

Chapman, D. C., Numerical treatment of cross-shelf open boundaries in a barotropic coastal model, *J. Phys. Oceanogr., 15*, 1060-1075, 1985.

Chen, C., and R. C. Beardsley, A numerical study of stratified tidal rectification over finite-amplitude banks, I, Symmetric banks, *J. Phys. Oceanogr., 25*, 2090-2110, 1995.

Chen, C., R. O. Reid, and W. D. Nowlin, Jr., Near-inertial oscillations over the Texas- Louisiana shelf, *J. Geophys. Res., 101*, 3509-3524, 1996.

Csanady, G. T., Barotropic current over the continental shelf, *J. Phys. Oceanogr., 4*, 357-371, 1974.

Galperin, B., L. H. Kantha, S. Hassid, and A. Rosati, A quasi-equilibrium turbulent energy model for geophysical flows, *J. Atmos. Sci., 45*, 55-62, 1988.

Large, W.S., and S. Pond, Open ocean momentum flux measurements in moderate to strong winds, *J. Phys. Oceanogr., 16*, 1076-1084, 1981.

Mellor, G. L., and T. Yamada, A hierarchy of turbulence closure models for planetary boundary layers, *J. Atmos. Sci., 33*, 1791-1896, 1974.

Mellor, G. L., and T. Yamada, Development of a turbulence closure model for geophysical fluid problem. *Rev. Geophys., 20*, 851-875, 1982.

Millot, C. and M. Crepon, Inertial oscillations on the continental shelf of the Gulf of Lions: Observations and theory, *J. Phys. Oceanogr., 11*, 639-657, 1981.

Mooers, C. N. K., Several effects of a baroclinic current on the cross-stream propagation of inertial-internal waves, *Geophys. Astrophys. Fluid Dyn., 6*, 245-275, 1975a.

Mooers, C. N. K., Several effects of baroclinic currents on the three-dimensional propagation of inertial-internal waves, *Geophys. Astrophys. Fluid Dyn., 6*, 277-284, 1975b.

Reid, R. O., and R. E. Whitaker, Numerical model for astronomical tides in the Gulf of Mexico: theory and application, 115 pp. *technical report,* Dep. of Oceanogr., Tex. A&M Univ., College Station, 1981.

Weller, R. A., The relation of near-inertial motions observed in the mixed layer during the JASIN (1978) experiment to the local wind stress and to the quasi-geostrophic flow field, *J. Phys. Oceanogr., 12*, 1122-1136, 1982.

Woods, T. M., Observations of near-inertial motions during the Nantucket Shoal flux experiment, M.S. thesis, 112 pp., Mass. Inst. of Technol./Woods Hole Oceanogr. Inst., Joint Program, Cambridge, Mass., 1987.

C.Chen and L. Xie, Department of Marine Sciences, The University of Georgia, Athens, GA 30602-2206

(Received August 31, 1995; revised September 13, 1996; accepted October 17, 1996.)